SMHI

No 103, Dec 2003

Reports Meteorology and Climatology

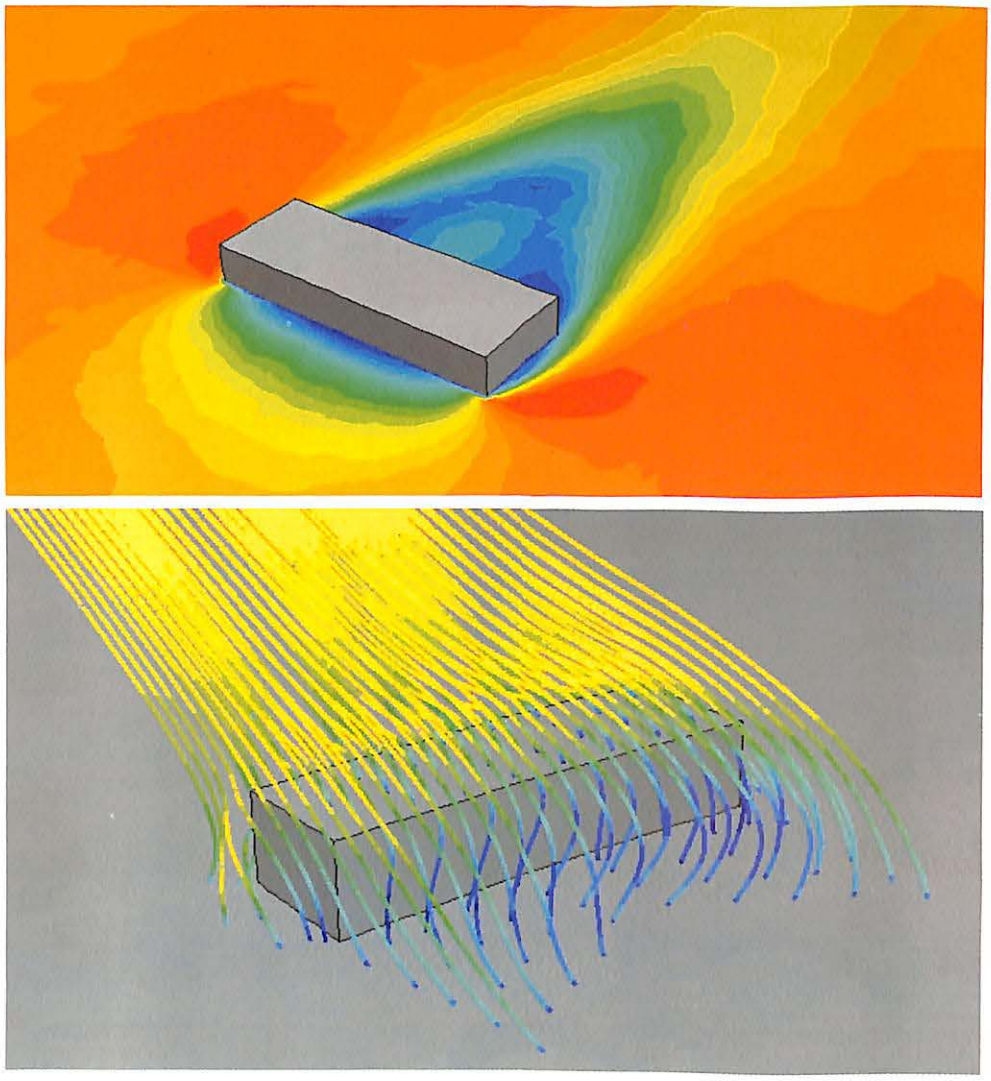

Numerical Quantification of Driving Rain on Buildings.

David Segersson

Cover: (upper figure) horizontal velocity field around a building.
(lower figure) raindrop trajectories around a building.

RMK
No 103, Dec 2003

Numerical Quantification of Driving Rain on Buildings.

David Segersson

Report Summary / Rapportsammanfattning

Issuing Agency/Utgivare	Report number/Publikation
Swedish Meteorological and Hydrological Institute S-601 76 NORRKÖPING Sweden	RMK No. 103
	Report date/Utgivningsdatum December 2003

Author (s)/Författare

David Segersson (david.segersson@smhi.se)

Title (and Subtitle/Titel

Numerical quantification of driving rain on buildings

Abstract/Sammandrag

Rain, which is given a horizontal velocity component by the influence of wind, is termed wind-driven or driving rain. Driving rain is one of the main sources to the amount of moisture a building is exposed to, and thereby contributes to the processes deteriorating the building envelope. Examples of damages to the building envelope that the onslaught of driving rain directly or indirectly can contribute to are: cracks caused by the freezing of water absorbed in the facade, mould or rot, corrosion of concrete reinforcements and soiling patterns. Knowledge about the exposure of a building to driving rain is needed in order to minimise the deteriorating processes, and thus contributes to ensure a satisfactory performance of the building design.

This work is meant as an introduction to the field of numerical quantification of driving rain on buildings. Focus is set on three-dimensional simulation of the wind flow and raindrop trajectories using CFD (Computational Fluid Dynamics). Interest is also paid to some specific properties of rainfall, such as drop size distributions and drag forces on raindrops. The study includes a detailed description of a method to calculate the driving rain distribution on a building, as well as application of the method to a rectangular facade. A qualitative evaluation of the results indicates that the method can be used to calculate the mean distribution of driving rain on simple geometries with sufficient accuracy.

Key words/sök-, nyckelord

CFD, driving rain, particle tracking, drop spectra, turbulent dispersion

Supplementary notes/Tillägg	Number of pages/Antal sidor	Language/Språk
	25	English

ISSN and title/ISSN och title

0347-2116 SMHI Reports Meteorology Climatology

Report available from/Rapporten kan köpas från:

SMHI
S-601 76 NORRKÖPING
Sweden

ABSTRACT

Numerical quantification of driving rain on buildings

David Segersson, Swedish Meteorological and Hydrological Institute, Folkborgsvägen 1, 601 76 Norrköping

Rain, which is given a horizontal velocity component by the influence of wind, is termed wind-driven or driving rain. Driving rain is one of the main sources to the amount of moisture a building is exposed to, and thereby contributes to the processes deteriorating the building envelope. Examples of damages to the building envelope that the onslaught of driving rain directly or indirectly can contribute to are: cracks caused by the freezing of water absorbed in the facade, mould or rot, corrosion of concrete reinforcements and soiling patterns. Knowledge about the exposure of a building to driving rain is needed in order to minimise the deteriorating processes, and thus contributes to ensure a satisfactory performance of the building design.

This work is meant as an introduction to the field of numerical quantification of driving rain on buildings. Focus is set on three-dimensional simulation of the wind flow and raindrop trajectories using CFD (Computational Fluid Dynamics). Interest is also paid to some specific properties of rainfall, such as drop size distributions and drag forces on raindrops. The study includes a detailed description of a method to calculate the driving rain distribution on a building, as well as application of the method to a rectangular facade. A qualitative evaluation of the results indicates that the method can be used to calculate the mean distribution of driving rain on simple geometries with sufficient accuracy.

Keywords: CFD, Driving rain, Particle tracking, drop spectra, turbulent dispersion

REFERAT

Numerisk kvantifiering av slagregn på byggnader

David Segersson, Sveriges Meteorologiska och Hydrologiska Institut, Folkborgsvägen 1, 601 76 Norrköping

Regn som ges en horisontell hastighetskomponent genom vindpåverkan benämns slagregn. Slagregn står för en stor del av den fukt som en byggnad utsätts för, och bidrar därmed till de nedbrytande processer som verkar på byggnadsskalet. Exempel på skador på byggnadsskalet som slagregn direkt eller indirekt kan bidra till är: sprickor orsakade av frysning av vatten absorberat i fasaden, mögel och röta, korrosion av betongförstärkningar, samt nedsmutsning av fasader. Kännedom om hur utsatt en byggnad är för slagregn behövs för att minimera effekten av de nedbrytande processerna som verkar på byggnadsskalet och bidrar därmed till att kraven på prestanda och hållbarhet uppfylls.

Denna studie är tänkt som en introduktion till området numerisk kvantifiering av slagregn på byggnader. Fokus sätts på tredimensionella beräkningar av vind och regndroppstrajektorier med hjälp av CFD (Computational Fluid Dynamics). Utrymme ges även åt vissa specifika egenskaper hos regn, såsom droppspektra och formmotstånd för regndroppar. Studien innehåller även en detaljerad beskrivning av en metod för beräkning av slagregnsfördelningen på en byggnad, samt tillämpning av metoden på en rektangulär fasad. En kvalitativ utvärdering av resultaten tyder på att metoden kan användas för att beräkna fördelningen av slagregn på enkla geometrier med tillräcklig noggrannhet.

Nyckelord: CFD, Slagregn, Partikelspårning, droppspektrum, turbulent dispersion

PREFACE

This work was made for SMHI (Swedish Meteorological and Hydrological Institute). Interest for the subject was raised by inquiries from two consultant firms regarding the distribution of driving rain on buildings. One of the inquiries concerned the distribution of driving rain on the Royal Palace in Stockholm. SMHI did not, at that time, have the capability to meet the requests from the consultant firms. Seeing this, a decision was made to do an introductory study on the possibilities to calculate the distribution of driving rain on buildings.

The main initiator to the project was Roger Taesler. Roger Taesler has also supported the work with the project through constructive discussions and ideas.

David Segersson, Norrköping, 2003-10

CONTENTS

1 INTRODUCTION

Knowledge about the microclimate is crucial in order to ensure a successful building design. Information about climate parameters such as exposure to wind and rainfall is an important basis for decisions concerning choice of materials, choice of location and design of the building envelope. Despite the fact that the contribution of driving rain to the processes deteriorating the building envelope has been known for a long time, it continues to cause major economical losses. The reasons might be changes in construction routines, the use of new and not properly tested materials and untraditional design. Several of the processes deteriorating the building envelope have the involvement of water in common. Water acts as an agent in mechanical, chemical and biological processes. Examples of mechanical deteriorating processes are erosion, caused by the onslaught of driving rain, and cracks in the facade caused by cycles of freezing and thawing. The chemical effects of water are mainly related to transport of pollutants into the facade, causing, for example, corrosion of concrete reinforcements, while mould or rot are examples of biological effects. The deteriorating processes often result in surface soiling patterns on the facade, showing the run-off ways of rainwater. Besides damaging the building envelope itself, water penetrating the envelope may cause an unhealthy indoor environment (Högberg, 2002).

The definition of driving rain is rain that is given a horizontal velocity component by the influence of wind. To be able to design buildings with a satisfactory durability and performance, knowledge is needed about the exposure of the building to driving rain. The driving rain load can be quantified using experimental, empirical or numerical methods. Measurements of driving rain are very site-specific, and are usually not performed at meteorological stations. This makes the practical use of experimental methods to quantify driving rain very limited. Empirical methods can provide a rough estimate of the average quantity of driving rain to be expected on buildings, but are insufficient to determine a more detailed picture of the spatial distribution. More detailed information can be obtained through the use of numerical methods (Blocken, Carmeliet & Hens, 2002).

This report is meant as an introduction to the field of numerical quantification of driving rain loads on buildings. The possibility to use numerical calculations of driving rain within consultant work is investigated and the needs for further research is surveyed. The report also includes an attempt to use the CFD-code FLUENT 6.1 together with Matlab to calculate driving rain on the facade of a building. Efforts were undertaken in order to minimize the computational times. To take a step in this direction, a statistical method is presented for the discretization of the raindrop size distribution.

2 THEORY

2.1 Empirical methods

There are many different approaches for empirical estimation of the amount of rain impinging on the facade of a building. In this paper attention is paid only to the most common method. When using empirical relations to calculate driving rain, difference is often made between the intensity of free driving rain, *i.e.* rain carried by the wind through a vertical plane in the undisturbed wind flow field, and the intensity of driving rain on the building envelope. It is generally assumed that the intensity of free driving rain, R_v [*mm/hr*], can be related to the intensity of rain falling through a horizontal plane, R_h, through:

$$R_v = \alpha U_r R_h^{\beta} \quad (1)$$

where U_r [m/s] represents the reference wind speed and α and β are empirical constants. The standard values of these constants are $\alpha=0.22$ and $\beta=0.88$ (van Mook, 2002). The free driving rain intensity can be transformed to the intensity of driving rain on a building, R_f, through the use of a factor, κ, defined by:

$$\kappa = \frac{R_f}{R_v} \quad (2)$$

The factor κ is a complicated function of raindrop size distribution, position on the facade and wind flow conditions. It has been pointed out that κ and α both depend on the drop size distribution, *i.e.* they are interdependent, which implies that it would be better to use one constant instead of two (van Mook, 2002).

Even though empirical methods are fast and easy to use, they are not given further notice in this report because of their inability to provide detailed information. For a more complete survey of empirical methods, see for example Blocken, Carmeliet & Hens (2002).

2.2 Numerical Methods

Numerical calculation of driving rain is usually made using CFD (Computational Fluid Dynamics). In recent years quite a few authors have used CFD to simulate rain falling on buildings, *e.g.* van Mook (2002), Blocken & Carmeliet (2000a, 2000b, 2002), Karagiozis, Hadjisophocleous & Cao (1997) and Choi (1993, 1994, 1997). Central to numerical calculation of driving rain is the concept of catch ratio, defined as:

$$\eta = \frac{R_f}{R_h} \quad (3)$$

Although there are some differences in the ways used to calculate catch ratios by the different authors, the basic strategy is the same and consists of the following steps:

1) Steady-state calculation of the wind flow field.

2) Calculation of trajectories for raindrops released in the wind flow field.

3) Calculation of catch ratios based on the raindrop trajectories.

The catch ratio depends on many factors: speed and direction of the wind, the raindrop size distribution, the position on the building envelope and the geometry of the surroundings. Through the use of the basic strategy above, it is possible to take all these dependencies into consideration.

2.2.1 Calculation of the wind flow field

The wind flow field is obtained by solving the Reynolds averaged Navier-Stokes equations numerically, using CFD software. The commercial CFD-code FLUENT has been used by Blocken & Carmeliet (2000a, 2002) and van Mook (2002), and was also used for the calculations presented in this report. In previous studies, calculations have been made in both

two and three dimensions. Because of the highly three-dimensional character of flow around buildings, the usefulness of two-dimensional models is limited. Therefore only the three-dimensional case is considered here. Since the trajectory calculations are based on the wind flow field, the accuracy of it is of crucial importance. The problems involved in wind flow calculations are mainly related to turbulence modelling. If closure is obtained using a k-ε turbulence model, the flow on the windward side of a building can be calculated to a satisfactory degree of accuracy, while larger discrepancies to measurements can be found on the leeward side (Murakami, 1992). Fortunately, considering that mainly the windward side is exposed to driving rain, the flow on the leeward side is of less importance. The use of a relatively simple turbulence model, such as different versions of the k-ε model, is therefore justified and has also been the choice for all mentioned previous studies. The details of wind flow calculations are here left out and reference is instead given to Blocken, Roels & Carmeliet (2003).

2.2.2 *Raindrop trajectories*

The calculation of the raindrop trajectories is performed using Lagrangian particle tracking. A large number of raindrops are released in the wind flow field and their trajectories are calculated by solving a force balance equation for each raindrop:

$$m_d \frac{d\vec{U}_d}{dt} = m_d \vec{g} - \frac{p}{8} \mu \, Re \, C_d(Re) d \left(\vec{U}_d - \vec{U} \right) \tag{4}$$

where m_d is the mass of the raindrop, $\vec{g}$ is the gravitational acceleration, μ is the dynamic viscosity, $\vec{U}_d$ is the drop velocity, $\vec{U}$ is the wind velocity, d is the drop diameter and $C_d(Re)$ is the drag coefficient, which is a function of the particle Reynolds number, Re. The definition of the particle Reynolds number is given in equation (5), where ρ represents the density of the air.

$$Re = \frac{\rho d \left| \vec{U}_d - \vec{U} \right|}{\mu} \tag{5}$$

In reality the fall of a raindrop is a dynamic process. The drag forces of the airflow on the raindrop causes the water inside the drop to circulate and the surface of the drop to oscillate with certain frequencies. Small drops, with a smaller diameter than ca 0.54 *mm*, can be thought of as spherical, while larger drops are deformed due to drag forces. The deformed raindrops develop flat bases. To be able to compare the size of a deformed raindrop with the size of a spherical raindrop, an equivalent diameter is used. The concept of equivalent diameter is defined as the diameter of a spherical raindrop with equal volume as the considered (non-spherical) raindrop (Pruppacher & Klett, 1978). For simplicity, the equivalent diameter of a raindrop will from here on be referred to as simply the drop diameter. The deformation of a raindrop causes the drag coefficient of the raindrop to change. The drag coefficient is defined by:

$$C_d \equiv \frac{D}{(?U^2/2)A_c} \tag{6}$$

where D represents the magnitude of the drag force and A_c is the area of the raindrop projected perpendicular to the flow. The drag coefficient also depends on the other mentioned

processes, such as circulation within the drop, oscillation of the drop surface *etc*. Each flow condition corresponds to a certain drag coefficient. Reynolds number is a non-dimensional parameter (defined in equation 5) corresponding to certain flow conditions. For raindrops falling at their terminal velocities in stagnant air the drag coefficient can be shown to be a function of the Reynolds number solely. To be able to find a general relationship for the drag coefficient, it has been assumed that this applies for accelerating and decelerating raindrops as well. The assumption is, besides being intuitively quite close to the truth, also to some extent justified by the fact that raindrops reach their terminal velocity fast and then travel at it most of the time. Pruppacher & Klett (1978) numerically calculated the distance a drop travels before it reaches 99% of terminal velocity when released from rest, and found for drops with d= 0.2, 0.5, 1.0, 2.0 *mm* that the distance is: 0.90, 5.4, 12.6, 19.8 *m* respectively.

Because of the complex dynamic processes involved, there is no sufficiently accurate analytical relationship between the drag coefficient and the Reynolds number. There are however, measurements of terminal velocities as a function of drop diameter, made by Gunn & Kinzer (1949). By fitting a curve to their data, a relationship between the drag coefficient and Reynolds number, including all relevant processes, can be achieved (Choi, 1993). The data of Gunn & Kinzer only covers Reynolds numbers between 1.8 and 3549. For Reynolds numbers lower than 0.01 the viscous forces are totally dominant and Stokes drag description can be used. In the Stokes regime the drag coefficient is $24/Re$. In the interval between 0.01 and 1.8, where both viscous and inertial forces are significant, a smooth transition from the data of Gunn & Kinzer to Stokes drag description is obtained by including a few data points in the Stokes regime when fitting a curve to the data of Gun & Kinzer. When drops reach a diameter larger than about 6 *mm* the drag forces overpower the surface tension and cause the drops to break up (Pruppacher & Klett, 1978). It is not completely certain however, that a smaller raindrop falling at greater speed relative to the surrounding air, and thus experiencing the same Reynolds number (about 3600), will break up as well. To account for the possibility of small drops experiencing Reynolds numbers larger than 3600, care is taken to ensure that the fitted curve continues in a reasonable way also for larger Re. A curve (see Figure 1) was fitted to the whole range of data. The fitted curve together with Stokes description of drag gives a relationship for the whole interval of interest:

$$C_d = \begin{cases} Re/24\,, & Re \le 10^{-1} \\ 10^{Y}\,, & Re > 10^{-1} \end{cases}$$

$$Y = A_0 + A_1 X + A_2 X^2 + \ldots + A_8 X^8$$

$$X = \log(Re) \qquad (7)$$

$$A_0 = 1.4114 \quad A_1 = -0.9058 \quad A_2 = 0.0847 \quad A_3 = 0.0233 \quad A_4 = -0.0034$$

$$A_5 = -0.0021 \quad A_6 = 8.3387 \cdot 10^{-5} \quad A_7 = 1.1488 \cdot 10^{-4} \quad A_8 = 1.1490 \cdot 10^{-5}$$

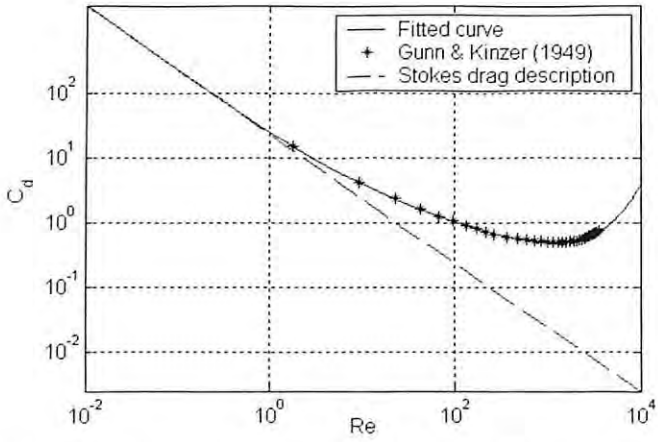

Figure 1. Relationship between Reynolds number and the drag coefficient of a raindrop. A curve has been fitted to the data of Gunn & Kinzer (1949) extended with Stokes description of drag.

2.2.3 *Raindrop size distribution*

Because of differences in mass and drag coefficients, drops of different sizes fall along different trajectories. Small drops are easily carried off by the wind, while larger drops are less influenced. In Figure 2, simulated trajectories for raindrops with diameters 0.5 and 4.0 *mm* are shown. It is clear from the figure that the smaller drops are more influenced than the larger ones. This variation with diameter, causes the catch ratio to be dependent of the raindrop size distribution (van Mook, 2002). The size distribution of raindrops usually stretches between a minimum drop diameter of 0.2 *mm* and a maximum drop diameter of 6.0 *mm*. As the drops fall through the air they collide. Collisions may cause drops to shatter or merge, and thus the raindrop size distribution changes continuously (Pruppacher & Klett, 1978). However, for the applications considered in this paper, *i.e.* driving rain on ground level, the drop size distribution is assumed to be constant.

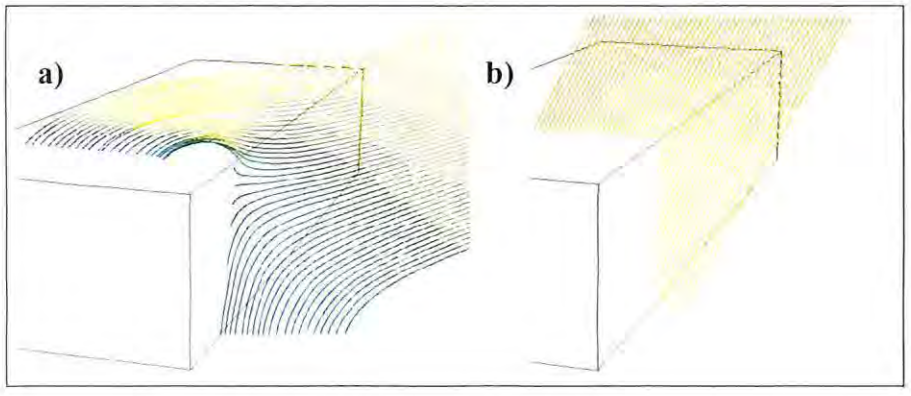

Figure 2. Trajectories for raindrops with a diameter of **a)** 0.5 *mm* and **b)** 4.0 *mm*. The raindrops were released along a line upstream of the building. The building is 22.1*m* long, 7.2 *m* wide and 4.3 *m* high. The reference wind speed is 5 m/s. The trajectories are given colours corresponding to their falling velocity, red represents higher velocities and blue lower.

The raindrop size distributions of individual rain events can vary significantly and may be correlated with many factors such as rainfall intensity, relative humidity and type of rain (orographic, thunderstorm, continuous etc.). The dependencies on all these factors have not been considered in this study, mainly because some of them are hard to handle numerically. The correlation between rainfall intensity and the drop size distribution can be handled numerically in a rather direct way, and is therefore investigated further. Expressions relating the raindrop size distribution to rainfall intensity have been given by a number of authors, *i.e.* Best (1950), Marshall and Palmer (1948) and Ulbrich (1983).

The drop size distributions are often given as mass concentration spectra, *m(d)*. A mass concentration spectrum gives the mass of water per volume of air for each drop diameter, [$kg\ m^{-3}m^{-1}$]. Van Mook (2002) summarizes these expressions in the following form:

$$m(d) = C_1 d^{C_2} e^{-C_3 d^{C_4}} \tag{8}$$

where *m(d)* is the mass concentration spectrum, *d* is the drop diameter [*m*] and the parameters C_1, C_2, C_3 and C_4 are given for the different expressions in Table 1.

A mass concentration spectrum can be modified to give the fraction of water in the air, *F(d)*, comprised of drops with a diameter smaller than *d*, through (van Mook, 2002):

$$F(d) = \frac{\int_0^d m(\Delta)\mathrm{d}\Delta}{\int_0^\infty m(\Delta)\mathrm{d}\Delta} \tag{9}$$

Table 1. Parameters for different mass concentration spectra summarized by equation (8).

	C_1	C_2	C_3	C_4	**Parameters**		
Marshall & Palmer (1948):	$10^3 \frac{\pi}{6} \rho_d n_0$	3	$10^3 \Lambda$	1		n_0 [$m^{-3}\ mm^{-1}$]	Λ [mm^{-1}] (R_h [$mm\ h^{-1}$])
					Standard values:	$8 \cdot 10^3$	$4.1 R_h^{-0.21}$
					Drizzle:	30 000	$5.7 R_h^{-0.21}$
					Widespread:	7 000	$4.1 R_h^{-0.21}$
					Thunderstorm:	1 400	$3.0 R_h^{-0.21}$

	C_1	C_2	C_3	C_4	**Parameters**		
Ulbrich (1983):	$10^{3+3\mu} \frac{\pi}{6} \rho_d n_0$	$\mu + 3$	$10^3 \Lambda$	1	n_0 [$m^{-3}\ mm^{-1}$]	Λ [mm^{-1}] (R_h [$mm\ h^{-1}$])	μ, [-]
					$8 \cdot 10^3$	$4.1 R_h^{-0.21}$	Realistic values between −1 and 6

	C_1	C_2	C_3	C_4	**Parameters**				
Best (1950):	$10^{-9+3b} \rho_d \frac{bCR_h^{q-ab}}{A^b}$	b-1	$\frac{10^{3b}}{A^b R_h^{ab}}$	B	A	a	b	C	q
					1.30	0.232	2.25	67	0.846

For the mass concentration spectrum given by Best (1950), solving equation (9) gives the expression:

$$F(d)=1-e^{-\left(\frac{d}{a}\right)^n},\ a=AR_h^p \tag{10}$$

where A, n and p are parameters with the averaged values 1.3, 2.25 and 0.232, respectively. From *F(d)* the PDF (Probability Density Function) can be calculated through:

$$f(d)=\mathrm{d}F/\mathrm{d}d=\frac{m(d)}{\int_0^\infty m(d)\mathrm{d}d} \tag{11}$$

When performing catch ratio calculations, the PDF for drops in a volume of air has to be modified to represent the PDF for the flux of drops through a horizontal plane. This is due to the variation of terminal velocity with drop diameter, and is done by multiplying the PDF with the terminal velocity. Thus the modified PDF, which from here on will be referred to as the flux PDF, can be obtained by (Blocken, 2000a):

$$f_h(d)=\frac{f(d)W_{term}(d)}{\int_d f(d)W_{term}\mathrm{d}d} \tag{12}$$

where $W_{term}(d)$ is the terminal velocity of raindrops in stagnant air. The terminal velocity of raindrops is obtained by the use of a relationship (Van Mook, 2002) based on a curve-fit to the data of Gunn & Kinzer (1949):

$$W_{term}=9.40\left(1-\exp\left(-1.57\cdot10^3 d^{1.15}\right)\right) \tag{13}$$

Examples of flux PDFs based on the drop size distribution of Best (1950) for different rain intensities can be seen in Figure 3a). To show how much variation there can be between the different drop size distributions given in Table 1, three different distributions are plotted in Figure 3b).

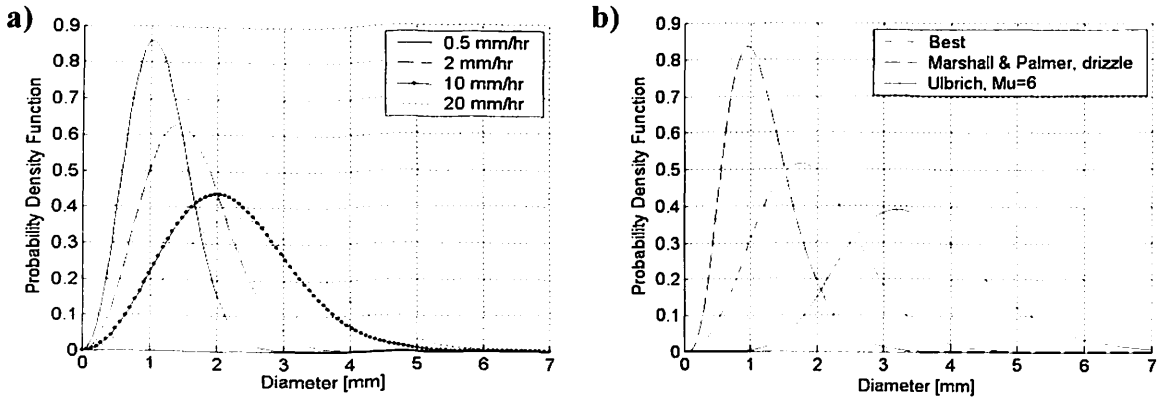

Figure 3. Probability density function of raindrops falling through a horizontal plane. The functions in **a)** are based on the drop size distribution of Best (1950) and the functions in **b)** are based on a rain intensity of 5.0 mm/hr.

2.2.4 *Discretization of the drop size distribution*

When performing numerical simulations, catch ratios for a number of different raindrop diameters are calculated. These catch ratios, which represent a single drop diameter, are called specific catch ratios, $\eta_d(d)$. By combining the specific catch ratios and weighting them according to their corresponding fractions in the raindrop size distribution, a global catch ratio, η, representing the whole drop size distribution can be obtained. When the drop size distribution is discretized by a large number of different drop diameters, as in Blocken & Carmeliet (2002) where 33 diameters are used, it is sufficient to multiply each specific catch ratio with the mass fraction represented by the corresponding drop diameter. To lower the number of needed simulations, a method is here proposed, which uses a more representative catch ratio for each mass fraction. The steps involved in the calculations can be outlined as:

1) Calculation of the specific catch ratios for a number of different drop diameters.

2) Dividing the drop size distribution into intervals based on the drop diameters for which specific catch ratios have been calculated in step 1).

3) Calculation of a representative drop diameter for each interval by taking the variation in the flux PDF and the variation of catch ratio with drop diameter into consideration.

4) Calculation of specific catch ratios corresponding to the representative drop diameters by linear interpolation between the specific catch ratios calculated in step 1).

5) Finally, the global catch ratio is obtained by weighting each specific catch ratio from step 4) with the corresponding fraction of the drop size distribution and summing.

The complete procedure can be expressed as:

$$\eta = \int_0^\infty f_h(d)\eta_d(d)\mathrm{d}d = \sum_{i=1}^{N} F_h^i \eta_{d,rep}^i$$
$$F_h^i = \int_{a_i}^{b_i} f_h(d)\mathrm{d}d \qquad (14)$$

where the index i refers to the diameter d_i for which the catch ratio has been calculated, N is the number of diameters and $\eta_{d,rep}^i$ is the representative specific catch ratio. The different weights, F_h^i (step 5), are calculated by integrating the flux PDF over the interval $a_i < d_i < b_i$. The limits of the intervals (step 2) are chosen to include all the diameters that have d_i as nearest neighbouring simulated diameter. Examples of a drop size distribution divided into intervals can be seen in Figure 4. To demonstrate what influence each interval has on the global catch ratio, the intervals in Figure 4 are given heights corresponding to the value of F_h^i.

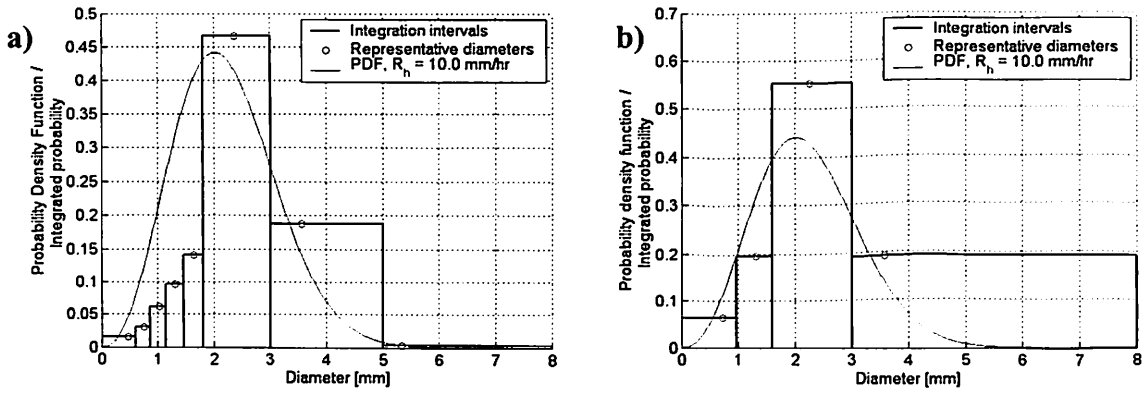

Figure 4. Discretizations of the drop size distribution based on simulated catch ratios for drop diameters **a)** 0.5, 0.7, 1.0, 1.3, 1.6, 2.0, 4.0 and 6.0 *mm* **b)** 0.7, 1.2, 2.0 and 4.0 *mm*. The distribution is divided into intervals given a height corresponding to the value of F_h^i. Integration gives the mass fraction of the raindrops falling through a horizontal plane for each interval.

In order to find the representative drop diameter for each interval (step 3), the flux PDF is weighted with the specific catch ratio:

$$f_{h,\,weighted}(d) = f_h(d)\eta_d(d) \tag{15}$$

Setting $\eta^i_{d,rep}$ as reference to the catch ratio causes the integral of $f_{h,weighted}$ over the interval i to be zero:

$$0 = \int_{a_i}^{b_i} f_{h,weighted}(d)\mathrm{d}d = \int_{a_i}^{b_i} f_h(\mathrm{d})[\eta(\mathrm{d}) - \eta^{\mathrm{i}}_{\mathrm{d,rep}}]\mathrm{d}d \tag{16}$$

Since η_d is not known for all drop diameters, it is assumed to vary linearly with the drop diameter over the integration intervals. The deviation in η_d from $\eta^i_{d,rep}$ in equation (16) can thereby be replaced by the deviation in d from d^i_{rep}:

$$0 = \int_{a_i}^{b_i} f_h(\mathrm{d})[\eta(\mathrm{d}) - \eta^{\mathrm{i}}_{\mathrm{d,rep}}]\mathrm{d}d \approx \int_{a_i}^{b_i} f_h(d)(d - d^i_{rep})\mathrm{d}d \tag{17}$$

Equation (17) is solved using an iterative procedure to find the value of d^i_{rep}. In Figure 4 the representative diameters are marked for each interval.

When the value of d^i_{rep} is known, the corresponding specific catch ratio, $\eta^i_{d,rep}$, can be found by linear interpolation between the calculated specific catch ratios (step 4):

$$\eta^i_{d,rep} \approx \alpha_i \eta^{i-1}_d + \beta_i \eta^i_d + \gamma_i \eta^{i+1}_d \tag{18}$$

where the values of the interpolation coefficients α_i, β_i and γ_i depend on the representative diameter according to:

$$\begin{aligned} &for\ d^i_{rep} \le d_i:\ \alpha_i = 1-\beta_i,\quad \beta_i = \left(\frac{d^i_{rep}-d_{i-1}}{d_i-d_{i-1}}\right),\quad \gamma_i = 0 \\ &for\ d^i_{rep} > d_i:\ \alpha_i = 0,\quad \beta_i = 1-\gamma,\quad \gamma_i = \left(\frac{d^i_{rep}-d_i}{d_{i+1}-d_i}\right) \end{aligned} \tag{19}$$

If the representative diameter is larger or smaller than all d_i, $\eta^i_{d,rep}$ is extrapolated by setting it equal to the closest calculated specific catch ratio, η^i_d (*i.e.* $\beta_i = 1$ and $\alpha_i = \gamma_i = 0$).

To make the final summation of weighted catch ratios computationally effective, the interpolation coefficients from all intervals are summed for each d_i giving:

$$\begin{aligned} &\eta = \sum_{i=1}^{N} F^i_h \eta^i_{d,rep} \approx \sum_{i=1}^{N} F^i_h w^i_h \eta^i_d \\ &w^i_h = (\gamma_{i-1} + \beta_i + \alpha_{i+1}) \end{aligned} \tag{20}$$

It is important to remember that the calculation of the representative catch ratio for each interval is based on the assumption that the catch ratio varies linearly with drop diameter. If simulations are made for very few diameters, especially in the interval 0.2-2.0 *mm* where most of the non-linearity in the catch ratio lies, this assumption might be too inaccurate.

2.2.5 *Turbulent dispersion*

The mean path of a raindrop is given by the mean wind flow field, gravity and the inertia of the raindrop. Wind turbulence can cause the raindrop to deviate from the mean path, and if close to a wall, drive the raindrop onto the wall. The deviation from the mean path due to turbulence is called turbulent dispersion. It is easy to relate to the effect of co-occurrence between wind gusts and rain. It is not evident though, how important the fluctuations in rain intensity due to wind gusts are when calculating the mean amount of driving rain.

A measure on how much a raindrop is dispersed, *i.e.* deviates from the mean path, is the stopping distance of the raindrop. The stopping distance is defined as the distance a raindrop travels after all driving forces have been taken away, and can be calculated from equation (4) using the initial conditions $g = 0$, $U_d(t < 0) = u_{initial}$ and $U(t \ge 0) = 0$ (for simplicity the initial conditions are expressed as scalars), giving the expression:

$$l_{stop} = \frac{4}{3} d \frac{\rho_d}{\rho} \int_0^{Re_i} \frac{dRe}{ReCd(Re)} \tag{21}$$

where $Re_i = \rho d u_{initial} / \mu$ (van Mook, 2002). The eddies causing the drop dispersion have a certain minimum dimension, L_{min}. Eddies with a dimension smaller than L_{min} does not significantly affect the raindrop trajectory. Van Mook (2002) assumes that L_{min} approximately equals l_{stop} and then uses the theory of the k-ε model to find the length scale of a turbulent eddie from the following relationship:

$$L_{turb.eddie} = C_{\mu}^{0.25} \kappa z \tag{22}$$

where C_{μ} is a numerical constant with the value 0.032 (Van Mook uses a non-standard value, the standard value is 0.09), κ is Von Karmans constant with the standard value 0.41 and z is the height above ground [m]. Equation (22) gives that $L_{turb.eddie} \approx 8$ m at a height of 50 m. Van Mook thereby concludes that at a wind speeds of 5 m/s, raindrops with diameters up to 2 mm, for which $L_{min} \approx l_{stop} \approx L_{turb.eddie}$, are influenced by the turbulence. It should be kept in mind that this result is based on the assumption that $l_{stop} \approx L_{min}$, and on the assumptions made in the k-ε model. The conclusion that can be drawn is that turbulent dispersion, at least for small raindrops, can be a significant factor. This conclusion is supported by Choi (1997), who investigated the influence of wind gusts on both the specific and the global catch ratio. He found that large gusts (lasting for three seconds) have a significant effect on the specific catch ratio for small drop diameters. It is important though, that the results of Choi also indicate that the effect is very limited when the whole drop size distribution is taken into account. It has been shown by Blocken & Carmeliet (2002) that the mean amount of driving rain can be calculated to a satisfying degree of accuracy without the inclusion of turbulent dispersion. They based their calculations on wind and rain data with a resolution of 10 minutes. The choice of 10 minutes data is motivated by the fact that this frequency is below most of the micrometeorological gust frequencies, and thus represents a mean situation.

Even though turbulent dispersion is recognised as a likely significant factor for the quantification of driving rain on buildings, it is not included in the calculations presented in this paper. There are two reasons for this. The first reason is that only the mean amount of driving rain is considered here. The second reason is that the inclusion of turbulent dispersion demands the use of a time-consuming statistical approach for catch ratio calculations (see section 2.2.6). While being important when considering extreme events, the inclusion of turbulent dispersion seems not to be needed for the mean situation.

2.2.6 *Procedures for calculation of catch ratios*

Two different methods for calculation of catch ratios can be found in literature. One of the two is a statistical method based on a "Monte Carlo"-approach. A large number of raindrops are released in the wind flow field and the number of raindrops per area in the release grid, N_h, is compared to the number of raindrops per area on a section of the surface of, for example, a building facade, N_f. This method can be expressed by the relation (van Mook, 2002):

$$\eta_d = \frac{R_f}{R_h} = \frac{N_f}{N_h} \tag{23}$$

The statistical method is easy to use and very flexible when it comes to handling complex geometries. It also allows the inclusion of turbulent dispersion in the trajectory calculations (see section 2.2.5). Unfortunately a very large number of released raindrops is required for equation (23) to be true. To find out how many raindrops that are needed for each run, repeated calculations with an increasing number of raindrops has to be made. The required number of raindrops for each run can then found by checking the convergence of the catch ratio. The work of van Mook (2002) shows that a number of raindrops in the order of 10^5-10^6 is needed to calculate specific catch ratios for 90 sections on a 45 m high and 169 m wide facade. To achieve a higher resolution in the results, a larger number of raindrops would be

needed. Considering also that trajectory calculations have to be made for many different drop diameters, and in some cases for many different wind conditions, the computational effort becomes overwhelming. To calculate catch ratios on computational cell basis, which would be very convenient, becomes far to time-consuming for anything except simple problems of very small scale using this method. However, the method can still be a good choice when it comes to calculating catch ratios on smaller areas or when a moderate resolution is required in the results.

The second method for the calculation of catch ratios is based on the conservation of mass. Assuming that the trajectory calculations are based on the mean wind field only, *i.e.* no turbulent dispersion is included, then each trajectory constitutes a streamline. If three raindrops are released in a wind flow field, their streamlines form a triangular stream tube (see Figure 5). The cross sectional area of the stream tube changes as it passes through the wind flow field and conservation of mass gives that the change in area is inversely proportional to the change in rain intensity,which can be expressed as:

$$\eta_d = \frac{R_f}{R_h} = \frac{A_h}{A_f} \tag{24}$$

where A_h is the horizontal area between the raindrops in the undisturbed flow field, and A_f is the area between the raindrops on a specified surface, *e.g.* the facade of a building. This approach only requires three raindrops to calculate the catch ratio of a zone on the building envelope, and thereby allows catch ratios with high spatial resolution to be obtained with a reasonable computational effort (Blocken & Carmeliet, 2002). Unfortunately, there are some disadvantages with this method as well. Very high accuracy is required in the trajectory calculations. To achieve this accuracy, a very fine mesh is needed in areas of high gradients in wind velocity, especially for drops with a diameter <1.0 *mm* which are very sensitive to wind influence. For complex geometries and large computational domains, the amount of cells required to give a satisfying accuracy might make the calculations quite time-consuming.

For the results presented in this study, the second method has been used. The details of the calculations are described in section 3.

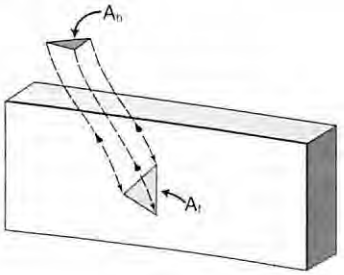

Figure 5. Three raindrop trajectories constituting a triangular stream tube. The cross-sectional area of the stream tube at release is called A_h and the area when the raindrops hit the facade is called A_f.

2.2.7 *Transient calculations*

Blocken & Carmeliet (2002, 2000a) calculate the amount of driving rain impinging on the facade of a building during a certain time period by linear interpolation between a limited number of steady-state simulations. By using a relationship such as that of Best (1950), to relate the rain drop size distribution to the rainfall intensity, a steady-state catch ratio for a given point on the facade can be defined for each combination of wind speed, wind direction and rainfall intensity. Since the catch ratio for any rainfall intensity can be obtained by combining the catch ratios for specific diameters, as described in section 2.2.4, the number of trajectory calculations for each wind flow field can be limited to a few diameters. In Figure 6 a structure of the needed simulations can be seen. For the details of the interpolation between the simulated catch ratios, reference is given to Blocken & Carmeliet (2000a).

To account for variations in wind speed, wind direction and rain intensity requires a large amount of CPU-time. Blocken & Carmeliet (2002) only consider winds perpendicular to the facade, and thereby limit the number of steady-state calculations to be made. Their catch ratio calculations are based on 33 different drop diameters and 10 wind speeds, *i.e.* 10 wind flow calculations and 330 trajectory calculations. The number of different drop diameters and wind speeds could probably be decreased, but still, if say four different wind directions, five wind speeds and eight drop diameters are to be considered, the number of simulations would be 20 wind flow calculations and 160 trajectory calculations. A possible way to lower the number of wind flow calculations would be to calculate one flow field for each wind-direction, and then scale the flow fields to get the different wind speeds for each direction. How this would affect the accuracy of the calculated catch ratios has not been investigated further in the current study.

To minimise the influence of turbulent dispersion and still keep a high temporal resolution, a suitable data sampling frequency is 10 minutes. All the needed data can be acquired from a standard meteorological station, measuring wind speed, wind direction and precipitation over 10 minutes intervals. By transforming data with a sampling frequency of 10 minutes to data with a lower frequency using a weighted averaging technique, it is possible to do transient calculations on, for example, one hour basis, without loosing to much accuracy (Blocken & Carmeliet, 2000b).

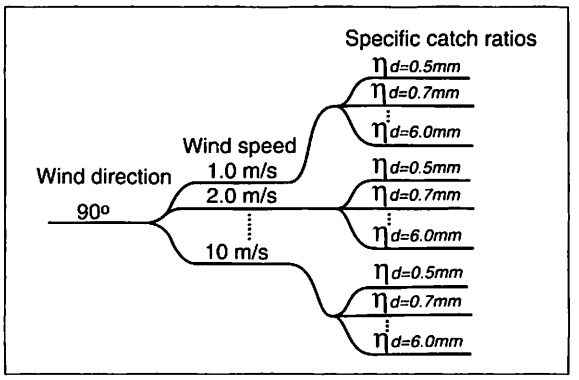

Figure 6. Structure of steady state simulations. A number of wind speeds are considered for all investigated wind directions, and catch ratios for a number of drop diameters are simulated for each wind speed. The number of diameters for each flow scenario has to be sufficient to linearize the variations in catch ratio with drop diameter.

3 IMPLEMENTATION

3.1 Performing trajectory calculations

Trajectory calculations were made using the same CFD-package as for the wind flow calculations, namely FLUENT 6.1. FLUENT calculates the trajectories by numerically integrating equation (4) with a trapezoidal scheme (Fluent, 2003). In FLUENT 6.1, general routines for particle tracking are implemented. These routines were altered to handle the specific properties of a falling raindrop. Calculations of the drag force for a raindrop can be made using the drag law of Morsi & Alexander (1971), which is included in FLUENT. This drag law is well suited for spherical raindrops, but underestimates the drag coefficient for larger and deformed raindrops. To be able to handle drops of all possible sizes, a function calculating the drag coefficient according to section 2.2.2 was implemented and linked to FLUENT. A comparison between the terminal velocities of raindrops falling in stagnant air measured by Gunn & Kinzer (1949) and velocities calculated with FLUENT together with the linked drag law can be seen in Figure 7.

Besides the drag-law, a function was also implemented to handle the injection of raindrops from a square grid into the wind flow field. When injecting raindrops, the initial vertical velocity component of the injected drops was set to the terminal velocity calculated by equation (13) and the initial horizontal velocity component was set to the wind speed at the level of release. When the raindrops impinge on a specified surface, *e.g.* a facade, a third function was executed which writes the coordinates of the raindrops to a file.

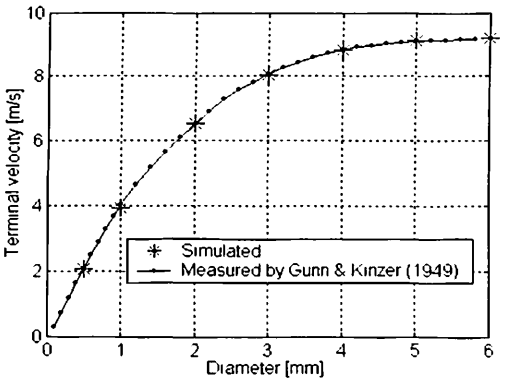

Figure 7. Comparison between terminal velocities of falling raindrops measured by Gunn & Kinzer (1949), and terminal velocities calculated with FLUENT 6.1, using a drag coefficient based on data of Gunn & Kinzer (1949) extended with relations of Pruppacher & Klett (1978) and Stokes law.

3.2 Calculations and post processing of catch ratios

The processing of the trajectory data and calculations of catch ratios were made using Matlab, version 6.5.0. The calculations were based on two data files written from FLUENT, one file containing the release coordinates of all raindrops and one file containing the coordinates of where the raindrops impinge on or fall through a specified surface, *e.g.* a facade. The calculations of catch ratios can be summarised by the following steps (Blocken, 2003):

1) Triangularization of the release grid. The coordinates from where the raindrops are released are divided into a set of triangles where the release coordinates constitute the corners. Figure 8c) shows a triangularized release grid with 400 raindrops.

2) The areas of the triangles built up by the raindrops are calculated at release and at the specified surface. The catch ratio is calculated from the areas by equation (24) and assigned to the triangles on the specified surface. Since the raindrops rarely fall directly on the edges of the specified surface, the fringe of the surface will not be covered by any triangles. This causes the catch ratio to be undefined in this area. See Figure 8a) for an example of results on a grid made up of triangles.

3) The grid on which the catch ratios from step 2) are defined is irregular and never the same for two different drop diameters. To be able to combine the specific catch ratios to a global catch ratio, all specific catch ratios have to be calculated on the same grid. The solution to this problem is to transfer the specific catch ratios from the triangular grid to a uniform grid. In order to do this, the catch ratios are first assigned to the triangle centroids, resulting in a set of scattered data points on the facade. The scattered data is then interpolated to the uniform grid using cubic splines. The catch ratios in the small area outside the triangle centroids are extrapolated using splines. See Figure 8b) for an example of catch ratios interpolated to a uniform grid and plotted as smoothed contours.

In this study, catch ratios have only been calculated for plane vertical and horizontal surfaces. The interpolation made to transfer the catch ratios to a uniform grid becomes increasingly complicated with the geometric complexity of the surface. For a curved surface the coordinates of the triangle centroids would have to be transformed to a plane surface (to be able to use a two-dimensional interpolation technique), interpolated, and then transformed back to the curved surface.

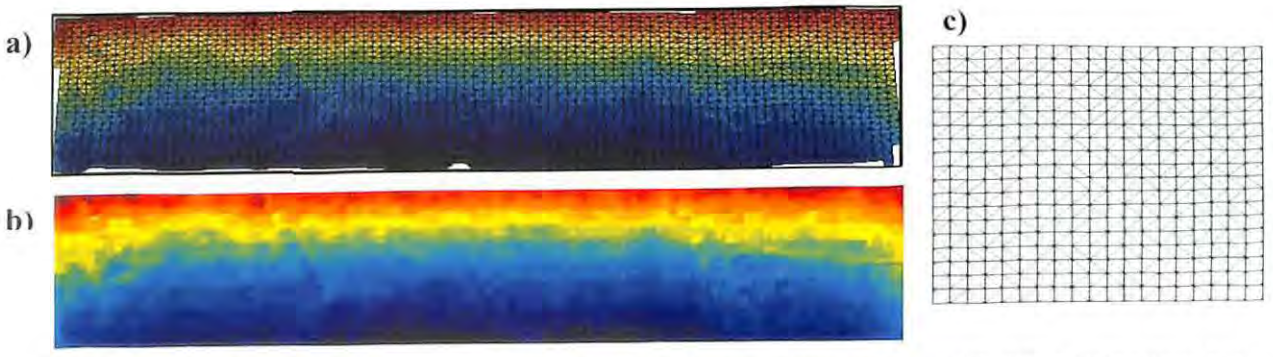

Figure 8. a) Calculated catch ratios showing an irregular pattern on a surface with data missing close to the edges.
b) Catch ratios interpolated to a regular grid and extrapolated to the edges.
c) Triangularization of a horizontal release grid based on 400 raindrops.

4 EVALUATION OF THE CALCULATION METHOD

Calculations of catch ratios were made for Fiskebäck Field Station, of Chalmers University, Sweden. The Field station is 22.1 *m* long, 7.2 *m* wide and 4.3 *m* high, and has the form of a rectangular box (Högberg, 2002). An unstructured hybrid mesh with approximately 1.5 million cells was used to discretisize a volume of 500·500·100 *m* for the calculations. The vicinity of the building was meshed using tetrahedral cells while the area further away from the building was meshed using hexahedral cells. Closest to the building the dimensions of the cells were between 0.05 and 0.5 *m*. The surface mesh around the building can be seen in Figure 9.

The wind flow field was calculated using a *k-ε realizable* turbulence model and standard wall-functions (Fluent, 2003). The flow around the building is showed in Figure 10a) and 10b). Based on the presence of expected flow features, such as the reverse flow on the roof of the building (Murakami *et al*, 1992), the density of the mesh and the used turbulence model were deemed sufficient to resolve the wind flow field.

Trajectory calculations were made for the south-west facade under the influence of wind with a reference speed of 5.0 *m/s* (at a height of 10 *m*) and a direction perpendicular to the facade. Simulations were made for drops with diameters 0.5, 0.7, 1.0, 1.3, 1.6, 2.0, 4.0 and 6.0 *mm*. A large number of raindrops were released outside the area influenced by the building, on a height of 12-50 *m*, depending on the diameter of the drops. The number of released drops for each drop diameter was between 10 000 and 25 000. The large number of particles was needed for a sufficient number of particles to impinge on the facade in areas of very small catch ratios. The resulting catch ratios can be seen in Figure 11.

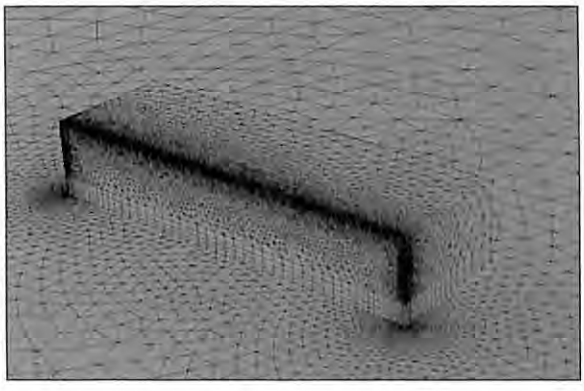

Figure 9. Unstructured tetrahedral surface mesh around the building. A dense mesh was used close to the edges of the building, where high velocity gradients and thereby also high catch ratios were expected.

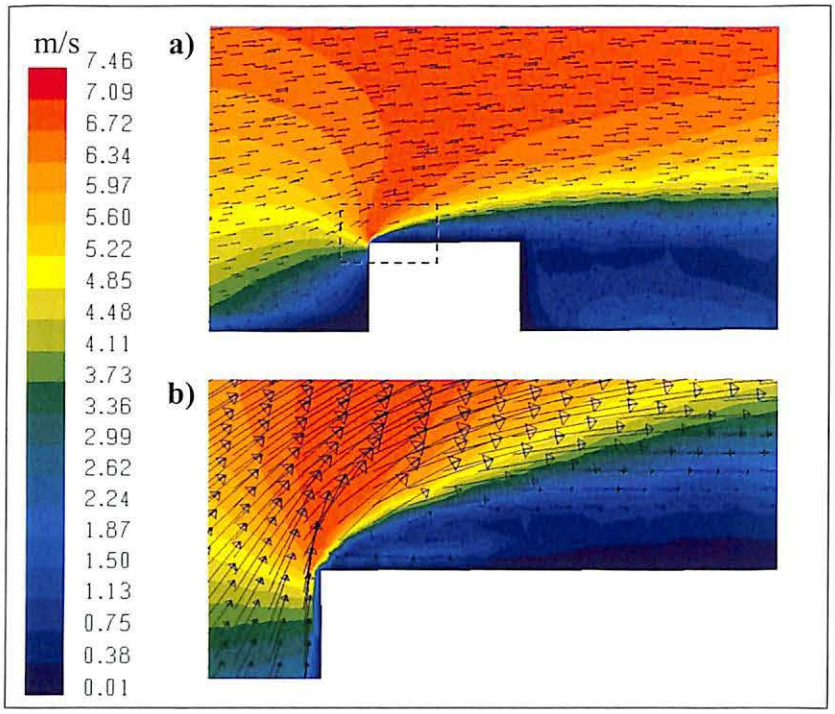

Figure 10. **a)** Wind flow field around the building at a reference wind speed of 5.0 *m*/s. The wind is directed perpendicular to the south-west facade.
b) Region of reverse flow on the roof.

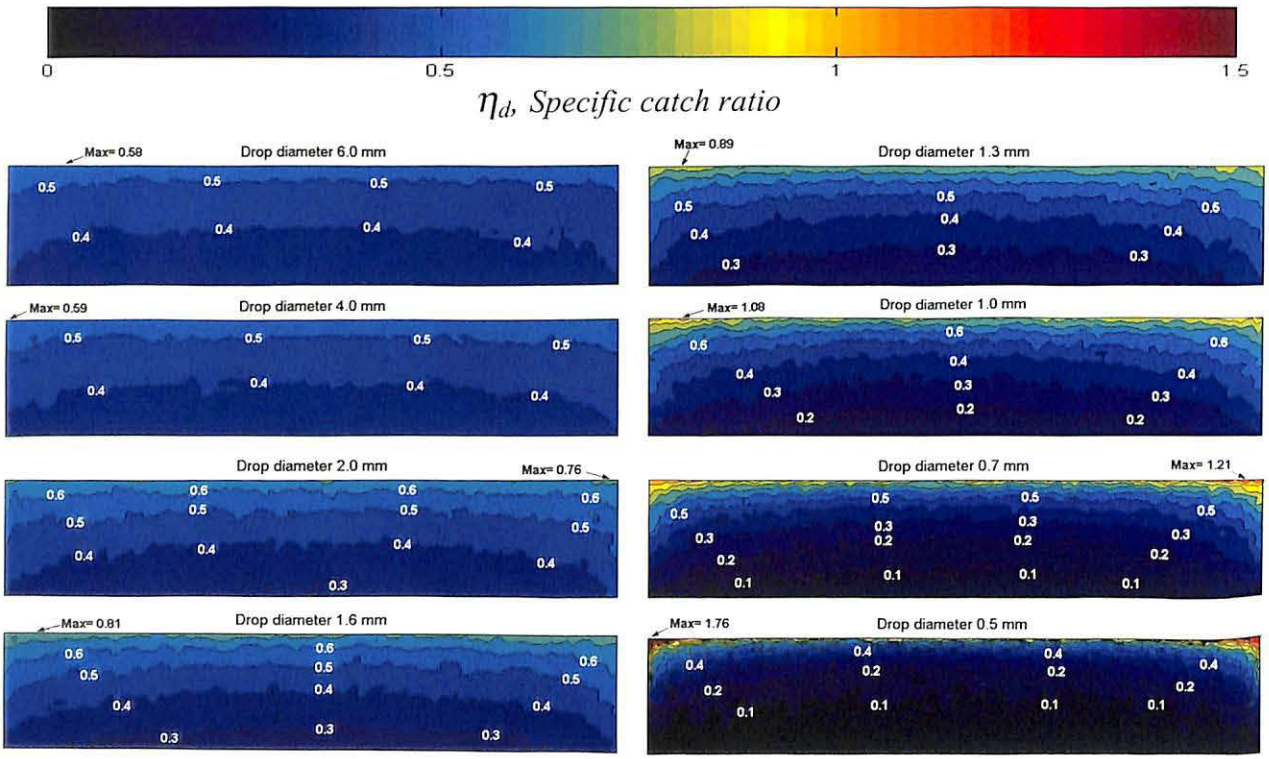

Figure 11. Specific catch ratios on the south-west facade of Fiskebäck Field station. The reference wind speed is 5.0 *m*/s and wind direction is south-west (perpendicular to the facade).

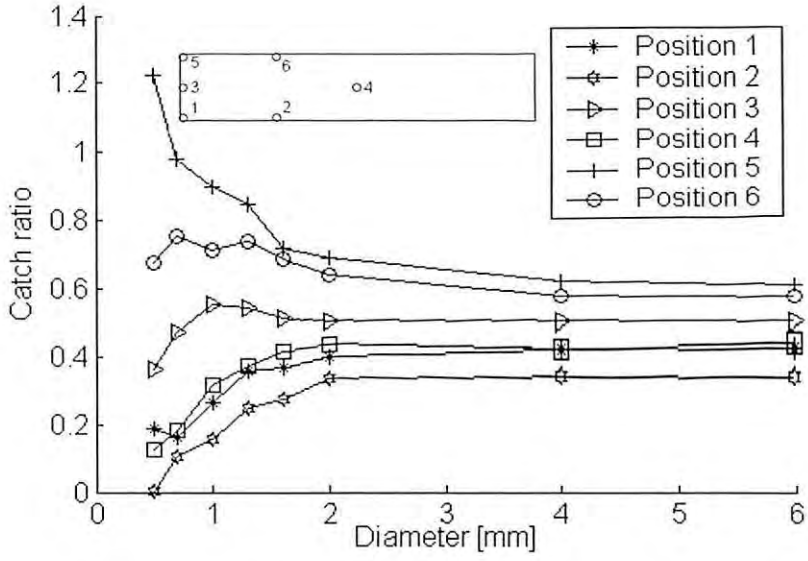

Figure 12. Dependence of the catch ratio on the drop diameter at five locations on the building facade.

The simulated diameters were chosen to represent the entire drop size distribution, as described in section 2.2.4. Simulations were made for eight different drop diameters. Most of the simulations were made for drop diameters smaller than 2.0 *mm*. This is because the catch ratio is most non-linear for small raindrops, and thus demands more simulations to be linearized. The dependence of the catch ratio on the drop diameter was examined for five locations on the building facade and can be seen in Figure 12.

The global catch ratio was calculated for the rainfall intensities 0.5, 2.0, 10 and 20 *mm/hr*, using the drop size spectrum given by Best (1950), and is presented in Figure 13. The flux PDFs on which the weighting of the specific catch ratios were based, can be seen in Figure 3a).

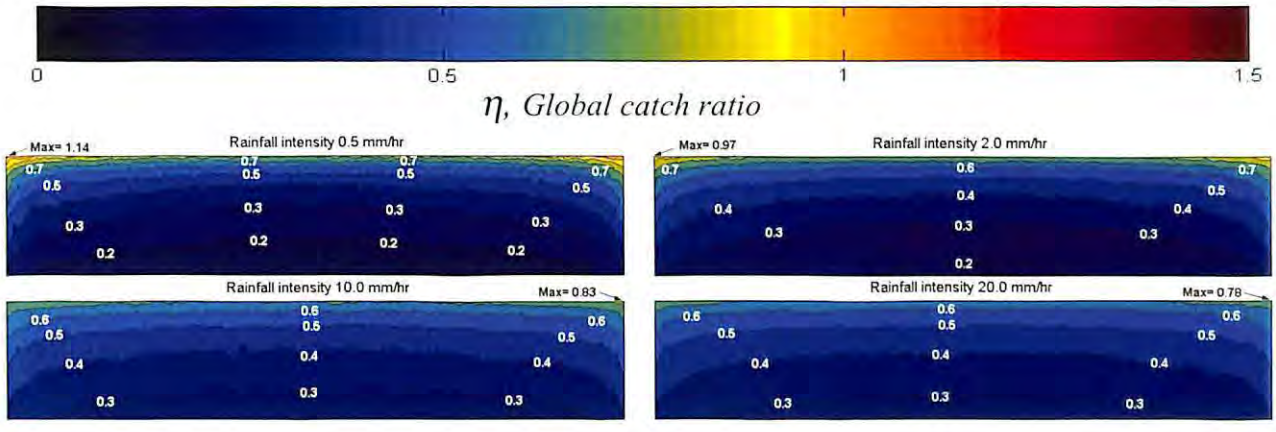

Figure 13. Catch ratios representative for the entire drop size distribution for different rainfall intensities.

5 DISCUSSION

It is known from field measurements that the intensity of driving rain on a facade is highest close to the upper edges of the building envelope. This is because the drag force from the air is overpowered by the raindrops inertia and gravity, which drives the raindrop out of the air stream and onto the wall. Around the edges of the building, where the acceleration in wind velocity is strongest, it is impossible for any but the smallest drops to follow the air stream. Thus, a large number of drops hit the facade close to the roof and the corners (Högberg, 2002). The results presented in Figure 11 and 13 show the expected features of the driving rain pattern, such as catch ratios increasing towards the edges. The irregularities that can be seen in catch ratios come from inaccuracies in the trajectory calculations and can be decreased by refining the mesh.

A qualitative comparison between the results presented in Figure 11 and catch ratios calculated for a similar building by Blocken & Carmeliet (2002) shows a close resemblance. The results of Blocken & Carmeliet have been verified by full-scale measurements, showing good agreement with measured amounts of driving rain. Considering that the calculations in this report was made using the same method as Blocken & Carmeliet, the catch ratios in Figure 11 and 13 can be thought to give a sufficiently accurate picture of the mean distribution of driving rain.

A problem when trying to obtain accurate catch ratios with sufficient resolution, are the long computation times. This especially applies for drops smaller than 0.5 *mm*, which are easily affected by wind drag and follow the wind flow very closely. To track a small drop in an area of high wind velocity gradients, a very fine mesh is required, which leads to time-consuming computations. The need for a very fine grid can probably to some extent be blamed on the integration scheme for particle tracking included in FLUENT. The scheme uses linear interpolation to get the air velocity at the particle location for every time step. If a higher order interpolation technique was used, the demands on the mesh could probably be lowered (at the cost of a slower tracking procedure).

The difficulties with tracking small raindrops had some influence on the choice of simulated raindrop diameters. The smallest raindrops, for which catch ratios have been included in the results, have a diameter of 0.5 *mm*. To calculate catch ratios for $d < 0.5$ *mm* with a sufficient accuracy, a finer mesh would have been needed. Since a finer mesh would mean extending the already long computation times, this option was not pursued. The influence of the exclusion of the raindrops with $d < 0.5$ *mm* on the results depends on the drop size distribution. For drop size distributions corresponding to rainfall intensities of 10.0 and 0.5 *mm/hr* and the drop size distribution given by Best (1950), the weighting factor for $\eta_{d=0.3}$ would be 0.0038 and 0.027 respectively. Thus the influence of $\eta_{d=0.3}$ would be very small for high rainfall intensities, and more important for lower intensities. However, for most applications the influence of drops with $d < 0.5$ *mm* could probably be considered neglectable.

6 CONCLUDING REMARKS

A method for quantification of driving rain on building envelopes, based on the technique used by Blocken & Carmeliet (2002), has been implemented and tested. The CFD-code FLUENT 6.1 was used for wind flow calculations and trajectory calculations and Matlab was used for the processing of trajectory data. The method was found to give satisfactory results.

The practical use of a method addressing the exposure to driving rain depends very much on the simplicity and the generality of the method. The tested method is useful for engineering purposes only when it comes to relatively simple buildings. The causes for this are:

- High requirements on accuracy in the particle calculations, demanding the use of a very fine mesh in areas of high wind velocity gradients.
- Difficulties with interpolation of the catch ratios on complex surfaces.
- Time-consuming procedure to calculate all the catch ratios needed to perform a transient calculation of the amount of driving rain impinging on a facade.

An example of a viable task would be to calculate the mean distribution of driving rain for the most exposed facade of a building under a few different flow conditions. The results could for example be used when designing different kinds of protective measures against driving rain.

Numerical calculations of rain intensity onto or through surfaces can also be used for other areas than to calculate the distribution of driving rain on building envelopes. The same methods as are used for buildings could, for example, be used to investigate the efficiency of precipitation meters for different parts of the drop size distribution. The computational demands would be greatly lowered, as only a single catch ratio for the opening of the precipitation meter is needed. Investigations on precipitation meters can thus be considered a realizable task for the future. It is also possible that the here tested methods can, with some modifications, be used for other particles than raindrops, *e.g.* snow, hail or sediment particles.

6.1 Further research

There is still a considerable amount of work needed within the field of numerical driving rain calculations. Since the calculations are very time-consuming, they are so far only applicable within research or when large economical interests are depending on the results. By developing an optimised and user-friendly tool for use together with a general CFD-code, the calculations could probably become much more cost-effective.

Further work is needed before the inclusion of turbulent dispersion can be used to increase the accuracy of driving rain calculations. The results of van Mook (2002) indicate that the use of a more advanced turbulence model when calculating the wind flow field might be needed not to overestimate the effect of turbulent dispersion close to walls. Since the inclusion of turbulent dispersion also demands a larger number of raindrops than when using the mean flow, the required computing resources are one of the major limiting factors. Considering the recent development of computer performance, the area of turbulent dispersion will probably see a quick progress.

As the temporal resolution of calculations can be increased by the inclusion of turbulent dispersion, the variations in catch ratio due to variations in the drop size distribution become more important. Empirical expressions relating the drop size distribution to the rainfall intensity, such as that of Best (1950), has shown to be sufficient for determining the mean distribution of driving rain. However, to calculate the extreme values of catch ratios it would probably be necessary to take the variations of the drop size distribution into consideration in some way.

Verification of numerical driving rain calculations has so far only been made by a few researchers (Blocken *et al*, 2001). For the future development of numerical calculations of driving rain, more studies with full-scale measurements, especially within the field of turbulent dispersion, is of imperative importance.

7 REFERENCES

Best, A.C. (1950), The size distribution of raindrops, *Quarterly Journal of the Royal Meteorological Society*, Vol. 76, pp. 16-36.

Blocken, B. (2003). *Personal Correspondence.*

Blocken, B., Roels, S., Carmeliet, J. (2003). A numerical study of wind nuisance for a high-rise building group, *To be presented at: Proceedings 2nd International Building Physics Conference, Leuven, Belgium, September 14-18, 2003.*

Blocken, B., Carmeliet, J. (2002). Spatial and temporal distribution of driving rain on a low-rise building, *Journal of Wind and Structures*, Vol. 5, pp 441-462.

Blocken, B., Carmeliet, J., Hens, H. (2002). Methods for the quantification of driving rain on buildings, *Presented at the ASHRAE annual meeting, Honolulu, Hawaii, June 22-26, 2002.*

Blocken, B, Van Mook, F.J.R, Hagentoft, C.-E., Carmeliet, J. (2001). A status report of numerical-experimental driving rain studies on 3 full-scale buildings, *Proceedings of the 3rd European and African Conference on Wind Engineering, Eindhoven, The Netherlands*, pp. 133-140.

Blocken, B, Carmeliet, J. (2000a). Driving rain on building envelopes-I. Numerical estimation and full-scale experimental verification, *Journal of Thermal Environment & Building Science*, Vol.24, pp. 61-85

Blocken, B, Carmeliet, J. (2000b). Driving rain on building envelopes-II. Representative experimental data for driving rain estimation , *Journal of Thermal Environment & Building Science*, Vol.24, pp. 89-110

Choi, E.C.C. (1993). Simulation of wind-driven rain around a building, *Journal of Wind Engineering and Industrial Aerodynamics*, Vol. 46&47, pp. 721-729.

Choi, E.C.C. (1994). Parameters affecting the intensity off wind-driven rain on the front face of a building, *Journal of Wind Engineering and Industrial Aerodynamics*, Vol. 53, pp. 1-17.

Choi, E.C.C. (1997). Numerical modelling of gust effect on wind-driven rain, *Journal of Wind Engineering an Industrial Aerodynamics*, Vol. 72, pp. 107-116

Fluent (2003). *User manual, version 6.1*. Fluent Inc.

Högberg, A. (2002). *Microclimate load: transformed weather observations for use in design of durable buildings,* Ph. D. Thesis, Dep. of Building Physics, Chalmers University of Technology.

Karagiozis, A., Hadjisophocleous, G., Cao, S. (1997). Wind-driven rain distributions on two buildings, *Journal of Wind Engineering and Industrial Aerodynamics*, Vol. 67-68, pp. 559-572

Marshall, J.S., Palmer, W. McK. (1948). The distribution of raindrops with size, *Journal of Meteorology*, Vol. 5, pp. 165-166.

Murakami, S., Mochida, A., Hayashi, Y., Sakamoto, S., (1992). Numerical study on velocity-pressure field and wind forces for bluff bodies by k-ε, ASM and LES, *Journal of Wind Engineering and Industrial Aerodynamics*, Vol. 41-44, pp. 2841-2852.

Pruppacher, H.R., Klett, J.D. (1978). *Microphysics of clouds and precipitation*, D. Reidel Publishing Company, Boston.

Ulbrich, W.C. (1983). Natural variations in the analytical form of the raindrop size distribution, *Journal of Climate and Applied Meteorology*, Vol. 22, No. 10, pp. 1764-1775.

Van Mook, F.J.R. (2002). *Driving rain on building envelopes*. Ph. D. Thesis, Faculty of Architecture, Planning and Building, Eindhoven University of Technology.

SMHIs publications

SMHI publishes six report series. Three of these, the R-series, are intended for international readers and are in most cases written in English. For the others the Swedish language is used.

Names of the Series	**Published since**
RMK (Report Meteorology and Climatology)	1974
RH (Report Hydrology)	1990
RO (Report Oceanography)	1986
METEOROLOGI	1985
HYDROLOGI	1985
OCEANOGRAFI	1985

Earlier issues published in serie RMK

1 Thompson, T., Udin, I., and Omstedt, A. (1974)
Sea surface temperatures in waters surrounding Sweden.

2 Bodin, S. (1974)
Development on an unsteady atmospheric boundary layer model.

3 Moen, L. (1975)
A multi-level quasi-geostrophic model for short range weather predictions.

4 Holmström, I. (1976)
Optimization of atmospheric models.

5 Collins, W.G. (1976)
A parameterization model for calculation of vertical fluxes of momentum due to terrain induced gravity waves.

6 Nyberg, A. (1976)
On transport of sulphur over the North Atlantic.

7 Lundqvist, J.-E., and Udin, I. (1977)
Ice accretion on ships with special emphasis on Baltic conditions.

8 Eriksson, B. (1977)
Den dagliga och årliga variationen av temperatur, fuktighet och vindhastighet vid några orter i Sverige.

9 Holmström, I., and Stokes, J. (1978)
Statistical forecasting of sea level changes in the Baltic.

10 Omstedt, A., and Sahlberg, J. (1978)
Some results from a joint Swedish-Finnish sea ice experiment, March, 1977.

11 Haag, T. (1978)
Byggnadsindustrins väderberoende, seminarieuppsats i företagsekonomi, B-nivå.

12 Eriksson, B. (1978)
Vegetationsperioden i Sverige beräknad från temperaturobservationer.

13 Bodin, S. (1979)
En numerisk prognosmodell för det atmosfäriska gränsskiktet, grundad på den turbulenta energiekvationen.

14 Eriksson, B. (1979)
Temperaturfluktuationer under senaste 100 åren.

15 Udin, I., och Mattisson, I. (1979)
Havsis- och snöinformation ur datorbearbetade satellitdata - en modellstudie.

16 Eriksson, B. (1979)
Statistisk analys av nederbördsdata. Del I. Arealnederbörd.

17 Eriksson, B. (1980)
Statistisk analys av nederbördsdata. Del II. Frekvensanalys av månadsnederbörd.

18 Eriksson, B. (1980)
Årsmedelvärden (1931-60) av nederbörd, avdunstning och avrinning.

19 Omstedt, A. (1980)
A sensitivity analysis of steady, free floating ice.

20 Persson, C., och Omstedt, G. (1980)
En modell för beräkning av luftföroreningars spridning och deposition på mesoskala.

21 Jansson, D. (1980)
Studier av temperaturinversioner och vertikal vindskjuvning vid Sundsvall-Härnösands flygplats.

22 Sahlberg, J., and Törnevik, H. (1980)
A study of large scale cooling in the Bay of Bothnia.

23 Ericson, K., and Hårsmar, P.-O. (1980)
Boundary layer measurements at Klock-rike. Oct. 1977.

24 Bringfelt, B. (1980)
A comparison of forest evapotranspiration determined by some independent methods.

25 Bodin, S., and Fredriksson, U. (1980)
Uncertainty in wind forecasting for wind power networks.

26 Eriksson, B. (1980)
Graddagsstatistik för Sverige.

27 Eriksson, B.(1981)
Statistisk analys av nederbördsdata. Del III. 200-åriga nederbördsserier.

28 Eriksson, B. (1981)
Den "potentiella" evapotranspirationen i Sverige.

29 Pershagen, H. (1981)
Maximisnödjup i Sverige (perioden 1905-70).

30 Lönnqvist, O. (1981)
Nederbördsstatistik med praktiska tillämpningar.
(Precipitation statistics with practical applications.)

31 Melgarejo, J.W. (1981)
Similarity theory and resistance laws for the atmospheric boundary layer.

32 Liljas, E. (1981)
Analys av moln och nederbörd genom automatisk klassning av AVHRR-data.

33 Ericson, K. (1982)
Atmospheric boundary layer field experiment in Sweden 1980, GOTEX II, part I.

34 Schoeffler, P. (1982)
Dissipation, dispersion and stability of numerical schemes for advection and diffusion.

35 Undén, P. (1982)
The Swedish Limited Area Model. Part A. Formulation.

36 Bringfelt, B. (1982)
A forest evapotranspiration model using synoptic data.

37 Omstedt, G. (1982)
Spridning av luftförorening från skorsten i konvektiva gränsskikt.

38 Törnevik, H. (1982)
An aerobiological model for operational forecasts of pollen concentration in the air.

39 Eriksson, B. (1982)
Data rörande Sveriges temperaturklimat.

40 Omstedt, G. (1984)
An operational air pollution model using routine meteorological data.

41 Persson, C., and Funkquist, L. (1984)
Local scale plume model for nitrogen oxides. Model description.

42 Gollvik, S. (1984)
Estimation of orographic precipitation by dynamical interpretation of synoptic model data.

43 Lönnqvist, O. (1984)
Congression - A fast regression technique with a great number of functions of all predictors.

44 Laurin, S. (1984)
Population exposure to SO and NO_x from different sources in Stockholm.

45 Svensson, J. (1985)
Remote sensing of atmospheric tempera-ture profiles by TIROS Operational Vertical Sounder.

46 Eriksson, B. (1986)
Nederbörds- och humiditetsklimat i Sverige under vegetationsperioden.

47 Taesler, R. (1986)
Köldperioden av olika längd och förekomst.

48 Wu Zengmao (1986)
Numerical study of lake-land breeze over Lake Vättern, Sweden.

49 Wu Zengmao (1986)
Numerical analysis of initialization procedure in a two-dimensional lake breeze model.

50 Persson, C. (1986)
Local scale plume model for nitrogen oxides. Verification.

51 Melgarejo, J.W. (1986)
An analytical model of the boundary layer above sloping terrain with an application to observations in Antarctica.

52 Bringfelt, B. (1986)
Test of a forest evapotranspiration model.

53 Josefsson, W. (1986)
Solar ultraviolet radiation in Sweden.

54 Dahlström, B. (1986)
Determination of areal precipitation for the Baltic Sea.

55 Persson, C. (SMHI), Rodhe, H. (MISU), De Geer, L.-E. (FOA) (1986)
The Chernobyl accident - A meteorological analysis of how radionucleides reached Sweden.

56 Persson, C., Robertson, L. (SMHI), Grennfelt, P., Kindbom, K., Lövblad, G., och Svanberg, P.-A. (IVL) (1987)
Luftföroreningsepisoden över södra Sverige 2 - 4 februari 1987.

57 Omstedt, G. (1988)
An operational air pollution model.

58 Alexandersson, H., Eriksson, B. (1989)
Climate fluctuations in Sweden 1860 - 1987.

59 Eriksson, B. (1989)
Snödjupsförhållanden i Sverige - Säsongerna 1950/51 - 1979/80.

60 Omstedt, G., Szegö, J. (1990)
Människors exponering för luftföroreningar.

61 Mueller, L., Robertson, L., Andersson, E., Gustafsson, N. (1990)
Meso-γ scale objective analysis of near surface temperature, humidity and wind, and its application in air pollution modelling.

62 Andersson, T., Mattisson, I. (1991)
A field test of thermometer screens.

63 Alexandersson, H., Gollvik, S., Meuller, L. (1991)
An energy balance model for prediction of surface temperatures.

64 Alexandersson, H., Dahlström, B. (1992)
Future climate in the Nordic region - survey and synthesis for the next century.

65 Persson, C., Langner, J., Robertson, L. (1994)
Regional spridningsmodell för Göteborgs och Bohus, Hallands och Älvsborgs län. (A mesoscale air pollution dispersion model for the Swedish west-coast region. In Swedish with captions also in English.)

66 Karlsson, K.-G. (1994)
Satellite-estimated cloudiness from NOAA AVHRR data in the Nordic area during 1993.

67 Karlsson, K-G. (1996)
Cloud classifications with the SCANDIA model.

68 Persson, C., Ullerstig, A. (1996)
Model calculations of dispersion of lindane over Europe. Pilot study with comparisons to measurements around the Baltic Sea and the Kattegat.

69 Langner, J., Persson, C., Robertson, L., and Ullerstig, A. (1996)
Air pollution Assessment Study Using the MATCH Modelling System. Application to sulfur and nitrogen compounds over Sweden 1994.

70 Robertson, L., Langner, J., Engardt, M. (1996)
MATCH - Meso-scale Atmosperic Transport and Chemistry modelling system.

71 Josefsson, W. (1996)
Five years of solar UV-radiation monitoring in Sweden.

72 Persson, C., Ullerstig, A., Robertson, L., Kindbom, K., Sjöberg, K. (1996)
The Swedish Precipitation Chemistry Network. Studies in network design using the MATCH modelling system and statistical methods.

73 Robertson, L. (1996)
Modelling of anthropogenic sulfur deposition to the African and South American continents.

74 Josefsson, W. (1996)
Solar UV-radiation monitoring 1996.

75 Häggmark, L., Ivarsson, K.-I. (SMHI), Olofsson, P.-O. (Militära vädertjänsten). (1997)
MESAN - Mesoskalig analys.

76 Bringfelt, B, Backström, H, Kindell, S, Omstedt, G, Persson, C, Ullerstig, A. (1997)
Calculations of PM-10 concentrations in Swedish cities- Modelling of inhalable particles

77 Gollvik, S. (1997)
The Teleflood project, estimation of precipitation over drainage basins.

78 Persson, C., Ullerstig, A. (1997)
Regional luftmiljöanalys för Västmanlands län baserad på MATCH modell-beräkningar och mätdata - Analys av 1994 års data

79 Josefsson, W., Karlsson, J.-E. (1997)
Measurements of total ozone 1994-1996.

80 Rummukainen, M. (1997)
Methods for statistical downscaling of GCM simulations.

81 Persson, T. (1997)
Solar irradiance modelling using satellite retrieved cloudiness - A pilot study

82 Langner, J., Bergström, R. (SMHI) and Pleijel, K. (IVL) (1998)
European scale modelling of sulfur, oxidized nitrogen and photochemical oxidants. Model development and evaluation for the 1994 growing season.

83 Rummukainen, M., Räisänen, J., Ullerstig, A., Bringfelt, B., Hansson, U., Graham, P., Willén, U. (1998)
RCA - Rossby Centre regional Atmospheric climate model: model description and results from the first multi-year simulation.

84 Räisänen, J., Döscher, R. (1998)
Simulation of present-day climate in Northen Europé in the HadCM2 OAGCM.

85 Räisänen, J., Rummukainen, M., Ullerstig, A., Bringfelt, B., Ulf Hansson, U., Willén, U. (1999)
The First Rossby Centre Regional Climate Scenario - Dynamical Downscaling of CO_2-induced Climate Change in the HadCM2 GCM.

86 Rummukainen, Markku. (1999)
On the Climate Change debate

87 Räisänen, Jouni (2000)
CO_2-induced climate change in northern Europé: comparison of 12 CMIP2 experiments.

88 Engardt, Magnuz (2000)
Sulphur simulations for East Asia using the MATCH model with meteorological data from ECMWF.

89 Persson, Thomas (2000)
Measurements of Solar Radiation in Sweden 1983-1998

90 Daniel B. Michelson, Tage Andersson
Swedish Meteorological and Hydrological Institute (2000)
Jarmo Koistinen, Finnish Meteorological Institute
Christopher G. Collier, Telford Institute of Environmental Systems, University of Salford
Johann Riedl, German Weather Service
Jan Szturc, Instiute of Meteorology and Water Management
Uta Gjertsen, The Norwegian Meteorological Institute
Aage Nielsen, Danish Meteorological Institute
Søren Overgaard, Danish Meteorological Institute
BALTEX Radar Data Centre Products and their Methodologies

91 Josefsson, Weine (2000)
Measurements of total ozone 1997 – 1999

92 Andersson, Tage (2000)
Boundary clear air echos in southern Sweden

93 Andersson, Tage (2000)
Using the Sun to check some weather radar parameters

94 Rummukainen, M.,S. Bergström, E. Källén, L. Moen, J. Rodhe, M. Tjernström (2000)
SWECLIM – The First Three Years

95 Meier, H. E Markus (2001)
The first Rossby Centre regional climate scenario for the Baltic Sea using a 3D coupled ice-ocean model

96 Landelius, Tomas, Weine Josefsson, Thomas Persson (2001)
A system for modelling solar radiation parameters with mesoscale spatial resolution

97 Karlsson, Karl-Göran (2001)
A NOAA AVHRR cloud climatology over Scandinavia covering the period 1991-2000

98 Bringfelt, B., Räisänen, J., Gollvik, S., Lindström, G., Graham, P., Ullerstig, A., (2001)
The land surface treatment for the Rossby Centre Regional Atmospheric Climate Model - version 2 (RCA2)

99 Kauker, Frank , Alfred Wegener Institute for Polar and Marine Research, Germany and Meier, H.E. Markus, Swedish Meteorological and Hydrological Institute, Rossby Centre, Sweden (2002)
Reconstructing atmospheric surface data for the period 1902-1998 to force a coupled ocean-sea ice model of the Baltic Sea.

100 Klein, Thomas., Bergström, Robert., Persson, Christer (2002)
Parameterization of dry deposition in MATCH

101 Räisänen, Jouni., Hansson U., Ullerstig A., Döscher R., Graham L P., Jones C., Meier M., Samuelsson P., Willén U (2003)
GCM driven simulations of recent and future climate with the Rossby Centre coupled atmosphere - Baltic Sea regional climate model RCAO

102 Persson, G. (2003)
Klimatmodellering och klimatscenarier från SWECLIMs synvinkel.

SAMMANFATTNING

MATCH-Sverige modellen utnyttjas bl.a. för kartläggning av den totala föroreningsdepositionen (frånsett dimdeposition) samt regionalskalig fördelning av lufthalter av svavel- och kväveföreningar över Sverige, samt för kvantifiering av Sveriges föroreningsbudget. Viss kartläggning av depositionen av baskatjoner görs också.

De största föroreningsdepositionerna erhålles varje år i sydvästra Götaland, på sydvästsidan av småländska höglandet. Depositionen minskar norrut, men Norrlands kustland har betydligt större föroreningsdeposition än Norrlands inland och fjälltrakter och detta förklaras bara delvis av större lokala svenska föroreningsbidrag längs Norrlandskusten. För perioden 1999-2002 ökar de svenska emissionerna från 5% till 7% av den totala depositionen av svavel till Sverige. För NO_x-kväve är motsvarande ökning av de svenska emissionerna från 11% till 13% av den totala depositionen och för ammoniumkväve ökar den från 14% till 17%. Anledningen till denna trend är att den totala depositionen minskar, medan det svenska bidraget är oförändrat.

Tidigare gjorda jämförelser har visat att MATCH-Sverige beräkningarna ger större - för ammoniumkväve nästan dubbelt så stor - totaldeposition till Sverige jämfört med den gamla EMEP-modellen. Jämförelser i denna studie visar att resultaten från MATCH-Sverige och EMEP's nya reviderade "Unified EMEP Eulerian model", som även baseras på reviderade emissionsdata (EMEP, 2003), stämmer väl överens för flertalet parametrar. Hittills har dock endast resultat från år 2000 publicerats för den nya reviderade EMEP-modellen.

För total svaveldeposition till Sverige ger MATCH-Sverige 5% större värden än EMEP, medan Sveriges svavelbidrag till den egna depositionen är 10% lägre i MATCH-Sverige beräkningarna trots att EMEP inte inkluderar sjöfartsbunkring i de svenska emissionerna. Total deposition av oxiderat kväve till Sverige är enligt MATCH-Sverige beräkningarna 15% lägre än den som EMEP-modellen ger, vilket är i motsats till resultaten från tidigare år. För Sveriges bidrag till den egna depositionen ger MATCH-Sverige ca 35% större deposition av oxiderat kväve än EMEP. Detta kan dock till en del förklaras av att sjöfartsbunkring ingår som svenska emissioner i MATCH-Sverige men inte i EMEP-beräkningarna. För total deposition av reducerat kväve till Sverige har skillnaderna minskat betydligt jämfört med tidigare år, men fortfarande ger MATCH-Sverige ca 50% större totaldeposition än EMEP-modellen. För Sveriges bidrag till den egna depositionen är MATCH-Sverige värdet dock endast 10% större än EMEP's resultat. Resultaten tyder på att den största delen av skillnaden i totaldeposition härstammar från olikheter i beräknade halter i luft och nederbörd som orsakas av den långväga föroreningstransporten. Skillnaderna är speciellt stora för Norrland och där är tillgången på mätdata för dataassimilation i MATCH-Sverige beräkningarna bristfällig.

En relativt tydlig samvariation erhålles mellan NAO-index och havssaltkoncentration i nederbörd i västra Sverige. För norra Bohuslän fås för den studerade perioden 1998-2002 en korrelationskoefficienten på drygt 0,7 och med den starkaste korrelationen under vintern.

SMHI

Swedish Meteorological and Hydrological Institute
SE-601 76 Norrköping Sweden
Tel +46 11 495 80 00 Fax +46 11 495 80 01

ISSN 0347-2116